ADVANCED FUNCTIONAL MATERIALS
www.afm-journal.de



# 3D-Printable Antimicrobial Composite Resins

*Jun Yue, Pei Zhao, Jennifer Y. Gerasimov, Marieke van de Lagemaat, Arjen Grotenhuis, Minie Rustema-Abbing, Henny C. van der Mei, Henk J. Busscher, Andreas Herrmann,* and Yijin Ren**

**3D printing is seen as a game-changing manufacturing process in many domains, including general medicine and dentistry, but the integration of more complex functions into 3D-printed materials remains lacking. Here, it is expanded on the repertoire of 3D-printable materials to include antimicrobial polymer resins, which are essential for development of medical devices due to the high incidence of biomaterial-associated infections. Monomers containing antimicrobial, positively charged quaternary ammonium groups with an appended alkyl chain are either directly copolymerized with conventional diurethanedimethacrylate/glycerol dimethacrylate (UDMA/GDMA) resin components by photocuring or prepolymerized as a linear chain for incorporation into a semi-interpenetrating polymer network by light-induced polymerization. For both strategies, dental 3D-printed objects fabricated by a stereolithography process kill bacteria on contact when positively charged quaternary ammonium groups are incorporated into the photocurable UDMA/GDMA resins. Leaching of quaternary ammonium monomers copolymerized with UDMA/GDMA resins is limited and without biological consequences within 4–6 d, while biological consequences could be confined to 1 d when prepolymerized quaternary ammonium group containing chains are incorporated in a semi-interpenetrating polymer network. Routine clinical handling and mechanical properties of the pristine polymer matrix are maintained upon incorporation of quaternary ammonium groups, qualifying the antimicrobially functionalized, 3D-printable composite resins for clinical use.**

## 1. Introduction

Over the past several years, additive manufacturing techniques, more commonly referred to as "3D printing" (3DP),[1] have entered the realm of public awareness by rapidly penetrating a variety of application areas beyond small-scale manufacturing and prototyping. Advancements in 3DP technology have also had an impact on drug delivery systems,[2–4] medical devices,[5,6] tissue engineering,[7–11] dental restorations,[12,13] microfluidics, and customized reactionware for chemical synthesis and analysis.[14,15] 3DP enables the low-cost, bottom-up fabrication of objects with complex geometries that are difficult to produce by traditional fabrication methods. Although 3D printed objects composed of metals, ceramics, polymers,[16] and even cell-loaded hydrogels have been realized,[17–19] the development of materials with integrated functions amenable for 3DP has been slow.

The surface properties of 3D printed materials are especially vital to their implementation in general medicine and dentistry, as nearly all medical devices have an interaction with the human body that occurs initially at the materials surface. Specifically, since many medical device surfaces attract microorganisms, engineering an intrinsic antimicrobial functionality in or onto implantable medical devices can reduce the risk of microbial infections associated with the presence of a foreign material in the human body.[20] Device-related infections pose major health threats and are currently the leading cause of failure of implanted devices. It has been estimated that at least 50% of all nosocomial infections are device-related and affect around two million patients each year in the United States alone.[21] Similarly, oral health is severely affected by the formation of infectious biofilms as many patients are unable to maintain sufficient oral hygiene using traditional means as tooth brushing or floss wire, especially when access to oral surfaces is hampered by, for instance, orthodontic appliances. Up to 15% of oral biofilm-related post-treatment complications in orthodontic patients require professional care with annual costs of over 500 million dollars in the United States.[22] Dental patients in the United States spend over 20 billion dollars annually to replace failed resin composite restorations that were damaged by bacterial infiltration and resulting secondary caries underneath a restoration.[23] Thus, motivated by the significant negative consequences of microbial biofilms in oral health and the highly individualized nature

Dr. J. Yue, Dr. P. Zhao, Dr. J. Y. Gerasimov, Prof. A. Herrmann
Zernike Institute for Advanced Materials
University of Groningen
9747 AG, Groningen, The Netherlands
E-mail: a.herrmann@rug.nl
Dr. J. Yue, M. van de Lagemaat, A. Grotenhuis, Prof. Y. Ren
Department of Orthodontics
University of Groningen and University Medical Center Groningen
9700 RB, Groningen, The Netherlands
E-mail: y.ren@umcg.nl
M. Rustema-Abbing, Prof. H. C. van der Mei, Prof. H. J. Busscher
Department of Biomedical Engineering
University of Groningen and University Medical Center Groningen
9713 AV, Groningen, The Netherlands

**DOI: 10.1002/adfm.201502384**

of customized intraoral appliances and prostheses calling for an all-digital workflow, we present a polymer design strategy to develop 3D printed, antimicrobial resins for manufacturing intraoral appliances and dental restorations. Design of antimicrobial resins is strongly preferred above surface coating of existing materials, as coating requires an additional step representing time and money in a clinical setting. Moreover, the design strategies presented are unique in the sense that they do not require any additional or even altered routines by the physicians involved. Application is not limited to dental or general medical ones, but can be transferred to other application areas where antimicrobial properties are desired.

Numerous efforts have been undertaken to equip conventional dental restorations with antimicrobial properties. These focused on release of various antibacterial agents such as fluorides,[24] zinc ions,[25,26] silver ions,[27] chlorhexidine,[28] and antimicrobial peptides.[29] However, the release of antimicrobial agents is always temporal and may impair the mechanical properties of the restorations or exert toxicity on the surrounding tissue if release is not properly controlled. Therefore, a material that functions through the mechanism of killing microorganisms on contact is a much more promising alternative. In several previous studies,[30–34] positively charged quaternary ammonium compounds have been covalently grafted onto surfaces to realize contact-killing effects against a variety of bacterial strains. Although their exact killing mechanism is still not fully elucidated, it is generally accepted that the grafted positively charged groups interact with the bacterial cell wall and disrupt the lipid membrane to release cytoplasmic constituents,[33] which causes cell death albeit through a different mechanism than utilized by positively charged compounds in solution.[35–37] Inspired by these studies, the aim of this study was to develop 3D printable, bacterial contact-killing resins that contain positively charged moieties and are compatible with stereolithographic, 3DP technologies. In addition, the cytotoxicity of possible leachables from the 3D printable materials developed was investigated using a method fine-tuned to dental application. 3D printable materials possessing complex functions, like the ability to kill adhering bacteria on contact, do not yet exist to the best of our knowledge. This is likely because it requires incorporation of a charged moiety into neutral resin components, minimization of leaching products, and adjustment of the rheological properties of the monomer mixture for 3DP at the same time, none of which is too trivial to achieve.

## 2. Results and Discussion

### 2.1. Synthesis Strategies and General Properties of the Resulting Materials

In the course of stereolithographic printing, a z-stage is moved in a liquid polymer resin tank and layer-by-layer photocuring provides one with a 3D object. Due to the outstanding geometry adaptability, different dental restorations can be easily fabricated in a single process just by changing the computer-aided design (CAD) drawing file. In the context of stereolithographic printing, rapid solidification of photopolymer liquid is an essential prerequisite for successful printing.[38] In this study, biocompatible diurethanedimethacrylate (UDMA) was selected as the frame component, which can be rapidly cross-linked by visible-light irradiation employing the widely used photosensitizer camphorquinone (CQ) in the presence of the coinitiator ethyl 4-dimethylaminobenzoat (EDMAB) (**Figure 1**a). To decrease the viscosity of UDMA, glycerol dimethacrylate (GDMA) was added as a cross-linkable "diluent" in proportion of 20–40 wt%. As an antimicrobial additive, we synthesized a series of quaternary ammonium-modified methacrylate monomers with different alkyl chain lengths ($n$ = 4, 8, 12, 16). Due to the presence of polymerizable methacrylate groups, the quaternary ammonium (QA_$C_n$) groups are covalently introduced into the polymer network by in situ copolymerization with the matrix resin components UDMA and GDMA (see also Figure 1a). Water contact angles on thus prepared polymers increased with increasing chain length for $n$ = 4–16 from 58° to 63°, 64°, and 68°, respectively.

Next, the surface atom compositions of the photocured resins were determined by X-ray photoelectron spectroscopy (XPS) upon incorporating QA_$C_{12}$ in the UDMA/GDMA matrix. As shown in Figure 1b, the appearance of an electron binding energy peak at 401.7 eV is indicative of the presence of quaternized nitrogen and supports the successful incorporation of positive charges into the cross-linked polymer matrix.[39] By adjusting the content of positively charged monomers before photocuring, the percentage of surface quaternized nitrogen in the afterward photocured material can be controlled (Figure 1c). Note that whereas the %N varied with increasing amounts of QA_$C_{12}$, the surface percentage of nitrogen at a binding energy of 401.7 eV, indicative of the presence of quaternized nitrogen, increased almost linearly with the QA_$C_{12}$ feed.

In another novel fabrication strategy that was motivated by minimizing leaching products from the resin, a high molecular weight, antimicrobial cationic polymer was incorporated in a semi-interpenetrating polymer network (SIPN) (**Figure 2**a), therewith trapping the positively charged macromolecule inside the cross-linked matrix. Such a material was realized in two steps: first, QA_$C_{12}$ monomers were converted into a QA-containing polymer (pQA) and mixed with the frame components for photocuring (Figure 2b). pQA was synthesized by copolymerization of cationic QA_$C_{12}$ monomers and 2-hydroxyethyl methacrylate (HEMA) employing the reversible addition-fragmentation chain-transfer (RAFT) polymerization. The comonomer was selected because it increases the compatibility with the frame components by binding to the ester and urethane groups within the cross-linked matrix through hydrogen bonding (see Scheme S1, Supporting Information). Before incorporation into the final resin, unreacted QA monomers and oligomers were removed through a simple precipitation and dialysis procedure. Analysis of the polymerization kinetics showed that the incorporation of the pQA_$C_{12}$ has no significant influence on the conversion of the matrix resin (Figure 2c). Trapping of pQA_$C_{12}$ (25 wt% pQA_$C_{12}$) in the SIPN resin was confirmed using XPS, showing the presence of 8 at% $N_{401.7\ eV}$, which is higher than obtained when copolymerizing QA_$C_{12}$ within a UDMA/GDMA resin. The thiocarbonylthio group at the end of the polymer chain (Figure 2a) may take part in the free-radical chain transfer

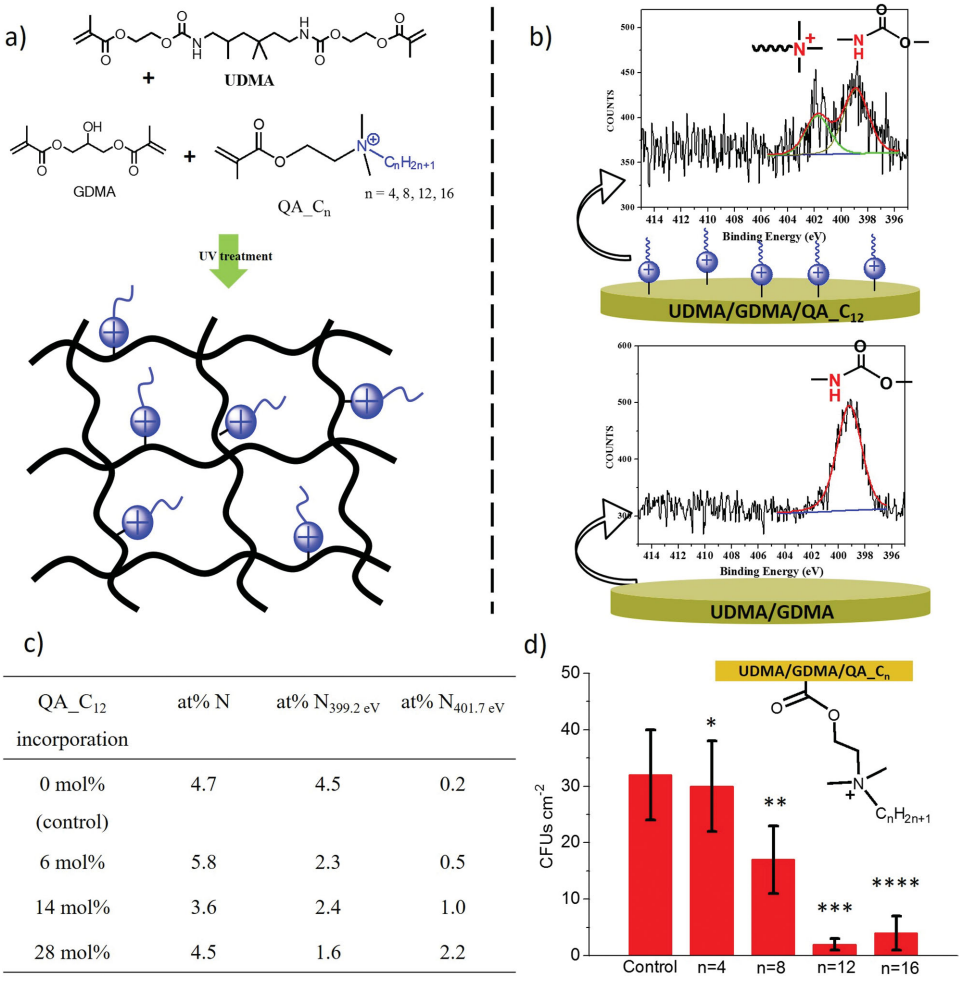


| $QA\_C_{12}$ incorporation | at% N | at% $N_{399.2\ eV}$ | at% $N_{401.7\ eV}$ |
|---|---|---|---|
| 0 mol% (control) | 4.7 | 4.5 | 0.2 |
| 6 mol% | 5.8 | 2.3 | 0.5 |
| 14 mol% | 3.6 | 2.4 | 1.0 |
| 28 mol% | 4.5 | 1.6 | 2.2 |

**Figure 1.** $QA\_C_n$ incorporated in a composite resin system. a) Structures of UDMA, GDMA, and $QA\_C_n$ monomers, and the incorporation of $QA\_C_n$ into the matrix resins; b) N1s electron binding energy peaks for UDMA/GDMA with 14 mol% $QA\_C_{12}$ and without $QA\_C_{12}$ (control) incorporated; and c) percentage surface nitrogen of UDMA/GDMA/$QA\_C_{12}$ resins with different feeds of $QA\_C_{12}$ obtained using XPS. The nitrogen peak was decomposed into two components of which the one at 401.7 eV is indicative of the presence of quaternized nitrogen; d) the number of CFUs per unit area (*S. mutans* NS) surviving contact with 14 mol% $QA\_C_n$ incorporated resins at a bacterial challenge concentration of ≈30 CFUs $cm^{-2}$. $^{*}p > 0.05$, $^{**}p < 0.05$, $^{***}p < 0.01$, and $^{****}p < 0.01$ as compared with a control (0 mol% $QA\_C_n$).

reactions during photocuring, leading to the covalent conjugation of $pQA\_C_{12}$ to the matrix resin (see Scheme S2, Supporting Information).

### 2.2. Biological Responses to Positively Charged Monomers Copolymerized in a Composite Resin

The bacterial contact-killing activities of solid $QA\_C_n$ containing resins were investigated by Petrifilm plate counting of colony forming units (CFUs) of bacteria after adhesion to the resins. To this end, we used Gram-positive *Streptococcus mutans*, a bacterial strain commonly found in the human oral cavity and a significant contributor to tooth decay.[40] The results (Figure 1d) showed that the length of the alkyl chain of the quaternized ammonium group has a significant ($p < 0.05$ for $n = 8$ and $p < 0.01$ for $n = 12$ and $n = 16$) influence on the contact-killing efficacy of the $QA\_C_n$ containing resins. Clearly, the killing efficacy increases with increasing alkyl chain length with an optimum for UDMA/GDMA/$QA\_C_{12}$. UDMA/GDMA/$QA\_C_4$ did not show any significant ($p > 0.05$) streptococcal killing compared to the control. Contrary to several other methods to determine bacterial contact killing, for instance, spray-coating[41] of a bacterial aerosol onto a surface, the Petrifilm plate counting system allows accurate determination of the bacterial challenge number. Bacterial challenge numbers used in this study range from 30 to 3000 CFUs $cm^{-2}$. This range comprises both challenge numbers coinciding with bacterial numbers per unit area expected to contaminate biomaterial implants and devices during surgical implantation[42] as well as challenge numbers of bacteria commonly found in early clinical biofilms as averages per unit area in the oral cavity. **Table 1** shows that the killing efficacy, i.e., the number of bacteria that are killed upon contact with the material divided by the challenge number, increases with increasing challenge numbers of streptococci for UDMA/GDMA/$QA\_C_{12}$, up to >99.99% at

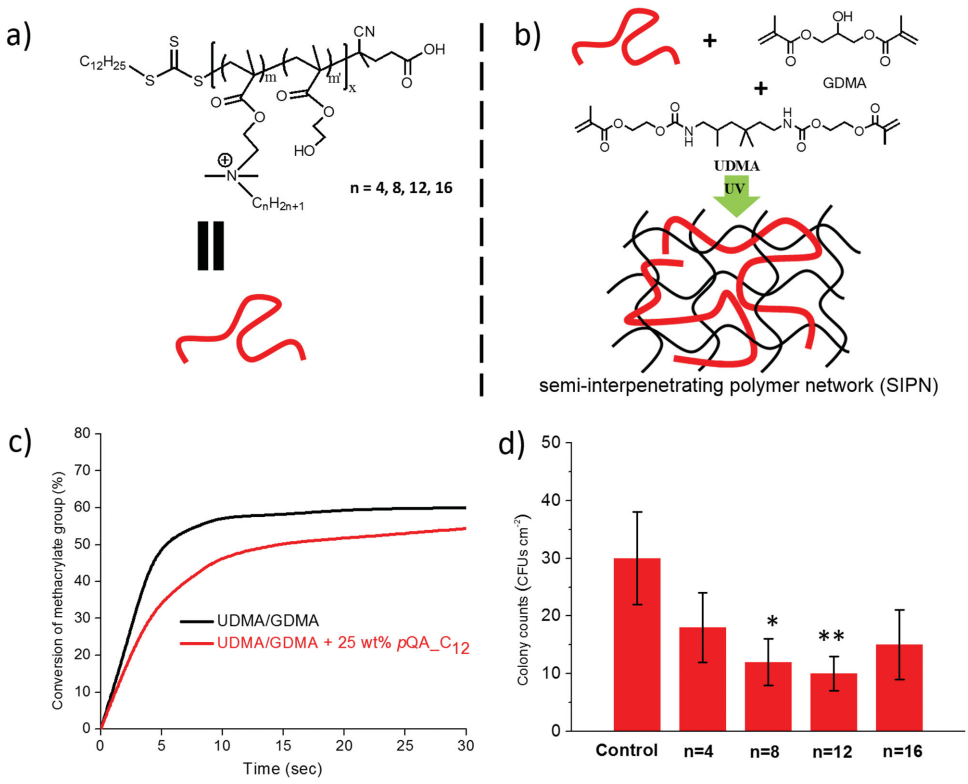


**Figure 2.** Semi-interpenetrating polymer network with QA_$C_n$ incorporated. a) Chemical structures of QA-containing polymers with different alkyl chain lengths; b) incorporation of pQA polymer into the SIPN resin forming a semi-interpenetrating polymer network; c) kinetics of photopolymerization of methacrylate groups in UDMA/GDMA with and without 25 wt% pQA_$C_{12}$, as derived from FTIR spectroscopy; and d) the number of CFUs per unit area (*S. mutans* NS) surviving contact with 25 wt% pQA_$C_n$ incorporated in a UDMA/GDMA resin at a bacterial challenge concentration of 30 CFUs cm$^{-2}$. $^{*}p < 0.01$, $^{**}p < 0.01$ as compared with a control (0 mol% pQA_$C_n$).

a challenge number of 3000 CFUs cm$^{-2}$. Note virtual absence of streptococcal contact killing by UDMA/GDMA without the QA_$C_{12}$ component (control). These results are in agreement with previous findings employing antimicrobial surfaces modified with quaternized ammonium coatings and polymers that are not 3D printable.[30,36,37]

Since in the oral cavity, materials are continuously bathed in saliva, salivary proteins will always adsorb before bacteria are able to adhere. This raises the important question of whether bacterial contact-killing materials still work after adsorption of a salivary protein film, generally called a "conditioning film." Therefore, streptococci were also allowed to adhere and contact UDMA/GDMA/QA_$C_{12}$ in presence of an adsorbed salivary conditioning film. In Table 1, it can be seen that the presence of a salivary film does not impede streptococcal contact killing. Previously,[43] the persistence of bacterial contact killing by hyperbranched quaternary ammonium coatings in presence of adsorbed protein films has been attributed to protein displacement underneath adhering bacteria by the pressure developing under the influence of the strong adhesion forces exerted by the positively charged coating upon the negatively charged bacteria.[44] In addition, it can be envisaged that bacterial enzymes degrade an adsorbed salivary protein film.

**Table 1.** The contact-killing efficacy of UDMA/GDMA and of UDMA/GDMA/QA_$C_{12}$ (14 mol%) in absence and presence of an adsorbed salivary conditioning film for different challenge numbers of *S. mutans* NS, obtained using the Petrifilm plate counting system. All data represent triplicate experiments with separate bacterial cultures and individually prepared materials.

| Material | 30 CFUs cm$^{-2}$ | 300 CFUs cm$^{-2}$ | 3000 CFUs cm$^{-2}$ |
|---|---|---|---|
| In absence of an adsorbed salivary conditioning film | | | |
| UDMA/GDMA | <1% | <0.1% | <0.01% |
| UDMA/GDMA/QA_$C_{12}$ | >99% | >99.9% | >99.99% |
| In presence of an adsorbed salivary conditioning film | | | |
| UDMA/GDMA | <10% | <1% | <0.1% |
| UDMA/GDMA/QA_$C_{12}$ | >99% | >99.9% | >99.99% |

### 2.3. 3D Printability and Biological Responses to Positively Charged Monomers Copolymerized in 3D Printed Composite Resin

Once the bacterial contact-killing ability of the quaternary ammonium containing UDMA/GDMA resin in absence and presence of an adsorbed salivary film was established, these materials were employed for 3D printing. For 3D printing, layer-by-layer photocuring is necessary, which possibly affects the tensile strength and bacterial contact-killing efficacy of the

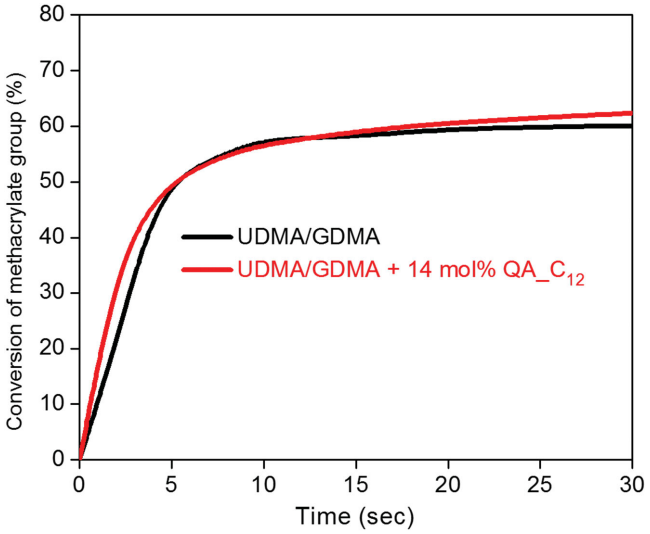


**Figure 3.** Kinetics of photopolymerization of methacrylate groups in UDMA/GDMA resins with and without 14 mol% QA_$C_{12}$, as derived from FTIR spectroscopy.

printed object. Therefore, we first established that the conversion rate of the methacrylate groups was not affected by the presence of QA_$C_{12}$ at 14 mol%. **Figure 3** confirms rapid polymerization (<10 s to reach higher than 55% conversion) in absence and presence of QA_$C_{12}$, which meets the needs of rapid curing required for stereolithographic printing.

A molar tooth model (**Figure 4**a, top) and a clear dental splint (Figure 4a, bottom) were successfully fabricated by subjecting a 14 mol% UDMA/GDMA/QA_$C_{12}$ formulation to 3D printing. In order to test the mechanical properties as well as the bacterial contact-killing efficacy of the 3D printed objects, dumbbell-shaped and disc-shaped objects were printed, respectively. Tensile tests of the 3D printed dumbbell-shaped bars were compared to test bars that were fabricated in a polymerization mold by conventional photoillumination. Both test bars exhibited very similar mechanical properties in tensile tests, as reflected in similar breaking stresses and breaking elongation values (Figure 4b). Thus, it can be concluded that CAD-sliced layers were fused together well during the layer-by-layer photocuring. Subsequently, the bacterial contact-killing efficacy was investigated employing the Petrifilm plate counting system to examine whether the bacterial contact-killing ability of the material was preserved after 3D printing. From the absence of colony forming units on the 3D printed, UDMA/GDMA/QA_$C_{12}$ disc as compared with the number of colony forming units on the UDMA/GDMA discs without QA_$C_{12}$, it can be concluded that the bacterial contact-killing ability of the material is preserved during 3D printing (Figure 4c). The long-term contact-killing ability of 3D printed objects was investigated by growing *S. mutans* biofilms on 3D printed discs. Confocal laser scanning microscopy (CLSM) after live/dead staining of 6 d old streptococcal biofilms on 3D printed UDMA/GDMA/QA_$C_{12}$ discs showed very little bacteria, that were in addition mostly dead when compared to 3D printed UDMA/GDMA discs without QA_$C_{12}$ (Figure 4d).

Leaching of unreacted monomer or QA_$C_{12}$, can not only affect the mechanism of bacterial killing but also the cytotoxicity of the material, although the requirement of absence of cytotoxicity depends largely on the application aimed for. In general, all composite resins demonstrate leakage of antibacterial and slightly cytotoxic components initially after photocuring. The degree of conversion of resin composites is never complete and ≈5%–10% of unpolymerized monomer can be extracted in water.[45] In **Figure 5**a it can be seen, that different components including QA_$C_{12}$, leach out of UDMA/GDMA/QA_$C_{12}$ discs in chemically detectable amounts when a volume of 10 mL of water is used as an elution fluid volume, but this does not necessarily imply biological consequences.

A proper design for experiments that demonstrate a biological significance of the leached amount of QA_$C_{12}$, is hard to make, as results can be greatly influenced by adjusting the elution fluid volume and the surface area of the material exposed. For maximal sensitivity, ultrahigh performance liquid chromatography–mass spectrometry (UPLC-MS) detection was applied with a small volume of 10 mL (Figure 5a). However, considering application of the present material in the oral cavity, only small surface areas of the material in the order of magnitude of 1 $cm^2$ will be exposed to saliva. The volume of saliva present in the human oral cavity is several mL's and is swallowed and replaced continuously during the day. Daily, between 1000 and 1400 mL of saliva is secreted by the different glands in the oral cavity.[46] Therefore, we based our experiments to investigate a possible biological significance of the amount of QA_$C_{12}$ leached out, on a total 24 h elution fluid volume of 100 mL (representing a tenfold "worst-case scenario"), immersing a UDMA/GDMA/QA_$C_{12}$ disc with a total surface area of 2 $cm^2$. Note that based on these considerations, our chemical detection assay represents a hundredfold "worst case scenario." Elution fluid was cellular growth medium and was replaced every 24 h, up to 6 d, using each daily volume for experiments. No zones of inhibition were observed around droplets of elution media placed on bacterially inoculated agar plates ("modified Kirby–Bauer test"),[47] demonstrating absence of microbiologically significant amounts of monomer or QA_$C_{12}$ leaching out over the course of minimally 6 d. In order to demonstrate possible cytotoxic effects, fibroblast cells were cultured in the elution media collected during different 24 h intervals. Fibroblasts are routinely used in cytotoxicity demonstration due to their high sensitivity to cytotoxic compounds. In Figure 5b, it can be seen that fibroblasts grow equally well with a similar morphology in 4 and 6 d elution medium as in growth medium. This implies that monomers leach out in cell-biologically significant amounts during the first 24 h of elution in 100 mL medium, but this release is highly temporary as common with composite resins, apart from the fact that we studied release in a tenfold "worst-case scenario."

### 2.4. Biological Responses to Prepolymerized Cationic Polymer Chains Incorporated into a Semi-Interpenetrating Polymer Network

Similar to the small molecule–based QA systems, contact killing with *S. mutans* NS of pQA (25 wt%) containing SIPN resins was evaluated. The pQA_$C_{12}$ containing SIPN

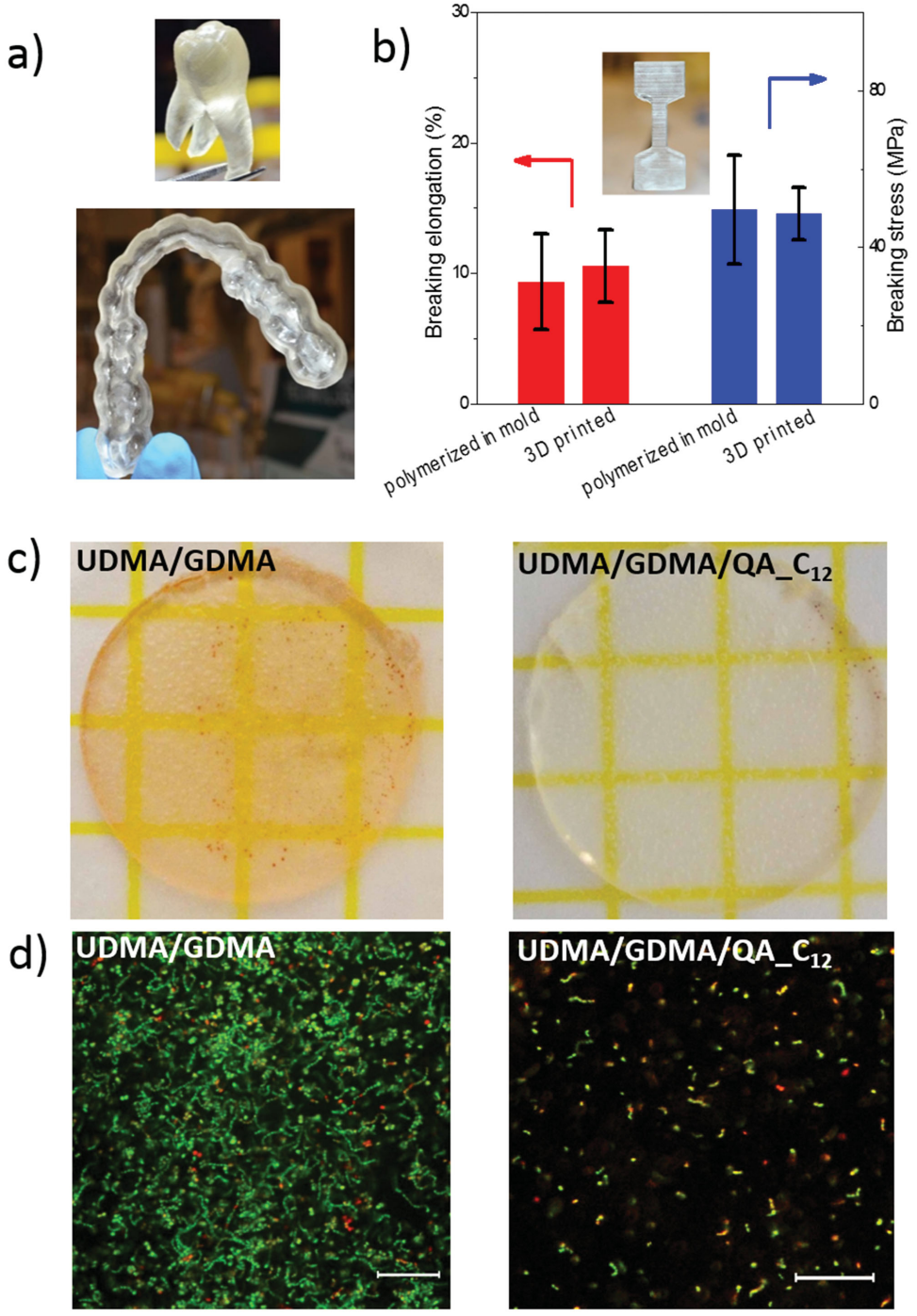


**Figure 4.** Object examples and properties of 3D printed UDMA/GDMA/QA_$C_{12}$: a) 3D printed model of a molar tooth model (top) and a clear dental splint (bottom); b) tensile properties of 14 mol% UDMA/GDMA/QA_$C_{12}$ 3D printed tensile test bar and a test bar prepared in a polymerization mold by conventional photoillumination; and c) comparison of the contact-killing efficacy of 3D printed UDMA/GDMA and UDMA/GDMA/QA_$C_{12}$ discs for *S. mutans* NS in the Petrifilm plate counting system (challenge number equals 30 CFUs $cm^{-2}$). Presence of CFUs (red dots) on the UDMA/GDMA disc versus the absence of colony forming units on the UDMA/GDMA/QA_$C_{12}$ disc indicates that the bacterial contact-killing ability of the material is preserved upon 3D printing; d) comparison of the long-term contact-killing efficacy of 3D printed UDMA/GDMA and UDMA/GDMA/QA_$C_{12}$ discs, demonstrated by CLSM after live/dead staining of 6 d old, *S. mutans* biofilms, grown in THB at 37 °C. Live bacteria are green fluorescent, while dead bacteria are red fluorescent. Bar markers indicate 50 µm.

exhibited the highest contact-killing efficacy toward *S. mutans* (Figure 2d) compared to the other alkyl chain lengths on the nitrogen center, as did UDMA/GDMA/QA_$C_{12}$. Differences between chain lengths were less pronounced, however, than for UDMA/GDMA/QA_$C_{12}$ (compare Figures 1b and 2d). Subsequently, the UDMA/GDMA/pQA_$C_{12}$ containing SIPN was

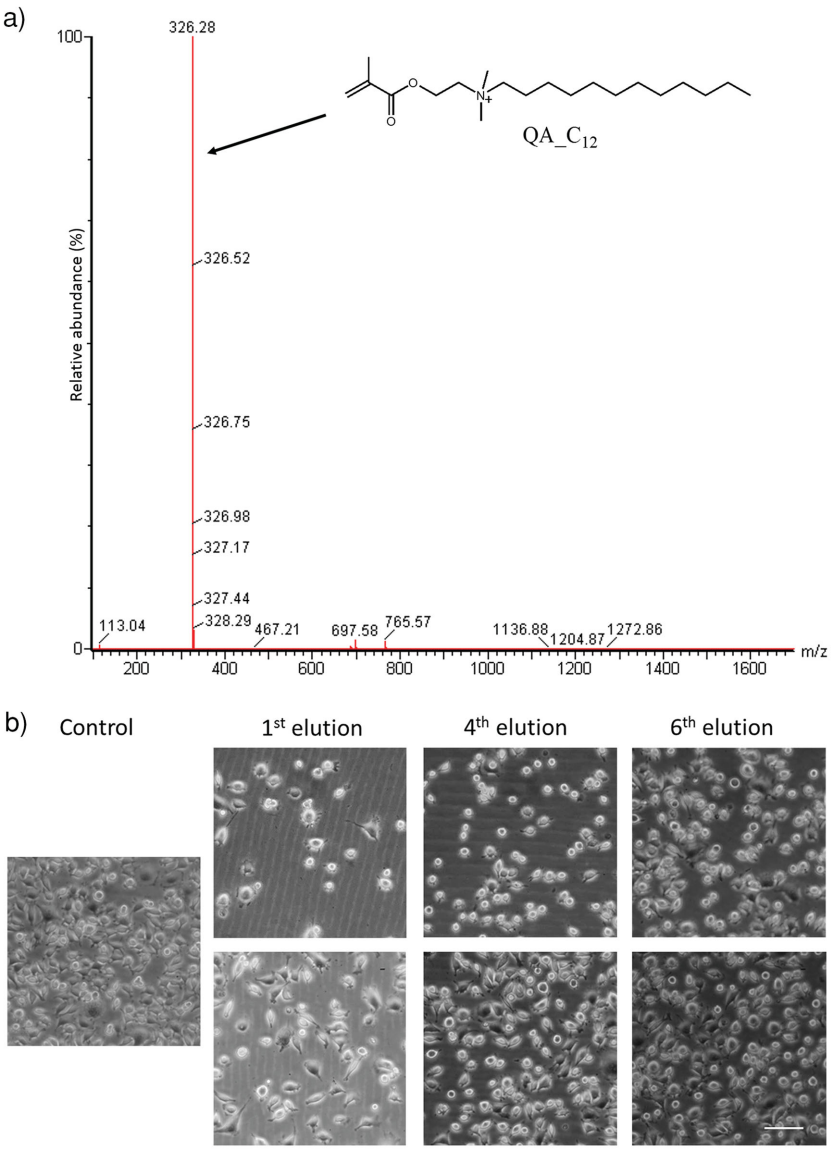


**Figure 5.** Leaching of QA_$C_{12}$ and effects on cytotoxicity; a) UPLC-MS detection of QA_$C_{12}$ (arrow) leached out of 1 $cm^2$ discs containing 14 mol% QA_$C_{12}$ immersed in 10 mL water for 6 d and b) morphology of fibroblast cells after growth in control medium (left panel) and in elution medium. Top row involves UDMA/GDMA discs and bottom row refers to UDMA/GDMA/QA_$C_{12}$ discs. Note initial effects of leached components on the morphology of the cells on both UDMA/GDMA and UDMA/GDMA/QA_$C_{12}$ discs with respect to the control. By comparison with the control, it can be seen that leakage of cytotoxic components, including possibly QA_$C_{12}$, occurs in cell-biologically negligible amounts within six elutions.

subjected to more extensive evaluation of its contact-killing ability and streptococcal challenge numbers were increased, while also the ability of the material to kill adhering streptococci upon contact in the presence of an adsorbed salivary film was evaluated (**Table 2**). Interestingly, bacterial contact killing by UDMA/GDMA/QA_$C_{12}$ in absence of a salivary conditioning film is similar as observed for UDMA/GDMA/pQA_$C_{12}$ (compare Tables 1 and 2), but in presence of a conditioning film, UDMA/GDMA/pQA_$C_{12}$ loses a couple of percentages in contact-killing efficacy despite the higher amount of quaternized nitrogen.

### 2.5. 3D Printability and Biological Responses to 3D Printed Prepolymerized Cationic Polymer Chains Incorporated into a Semi-Interpenetrating Polymer Network

Subsequently, 3D objects from pQA_$C_{12}$ containing UDMA/GDMA resin were printed. As shown in **Figure 6**a, different dental models and appliances were successfully fabricated by stereolithographic printing and their geometry and sizes were in accordance with the predetermined specifications. However, it was found that a material's compatibility with 3D printing was strongly dependent on the viscosity of the printing liquid. Printing was only successful when the content of the high-viscosity UDMA was above 40 wt%. Tensile properties of 3D printed test bars of pQA_$C_{12}$ containing UDMA/GDMA resin were similar as for UDMA/GDMA/pQA_$C_{12}$ fabricated in a polymerization mold (Figure 6b), although the material is considerably more brittle than UDMA/GDMA/QA_$C_{12}$ (compare Figures 4b and 6b). Moreover, also bacterial contact-killing efficacy of 3D printed discs made of pQA_$C_{12}$-containing UDMA/GDMA resin was fully preserved upon printing (Figure 6c).

UPLC-MS is a suitable method to chemically detect small molecules with a molecular weight of less than 5000 Da, but molecules with a higher molecular weight are difficult to detect. Accordingly, we attempted to detect pQA_$C_{12}$ from a UDMA/GDMA SIPN resin using UPLC-MS as done for QA_$C_{12}$ (see Figure 5a), but we observed no signals from pQA_$C_{12}$ in water. Therefore, we only carried out assays to establish the absence of biological consequences of possible leaching. As did UDMA/GDMA/QA_$C_{12}$, neither monomer nor pQA_$C_{12}$ leached out of UDMA/GDMA/pQA_$C_{12}$ in microbiologically significant amounts. However, by comparison with UDMA/GDMA/QA_$C_{12}$, the first elution from UDMA/GDMA/pQA_$C_{12}$ yielded a higher number of cells (compare Figure 5b with **Figure 7**). This confirms that leakage of pQA_$C_{12}$ from UDMA/GDMA/pQA_$C_{12}$ is reduced in a cell-biologically significant manner.

Several other compounds including, for instance, telechelic poly(2-oxazoline), have been used as additives to dental repair materials,[48] but materials were seldom evaluated for their ability to kill adhering bacteria upon contact in the presence of a salivary conditioning film. A quaternary ammonium methacryloxy silicate added to dental acrylic[49] was evaluated in the presence of an adsorbed salivary conditioning film and showed contact killing of an adhering *S. mutans* and *Actinomyces naeslundii* strain. Moreover, 24 h biofilm formation was

**Table 2.** The contact-killing efficacy of UDMA/GDMA (taken from Table 1) and of 25 wt% UDMA/GDMA/pQA_$C_{12}$ in an SIPN resin in absence and presence of an adsorbed salivary conditioning film for different challenge numbers of *S. mutans* NS, obtained using the Petrifilm plate counting system. All data represent duplicate experiments with separate bacterial cultures and individually prepared materials.

| Material | 30 CFUs $cm^{-2}$ | 300 CFUs $cm^{-2}$ | 3000 CFUs $cm^{-2}$ |
|---|---|---|---|
| In absence of an adsorbed salivary conditioning film | | | |
| UDMA/GDMA | <1% | <0.1% | <0.01% |
| UDMA/GDMA/pQA_$C_{12}$ | >99% | >99.9% | >99.9% |
| In presence of an adsorbed salivary conditioning film | | | |
| UDMA/GDMA | <10% | <1% | <0.1% |
| UDMA/GDMA/pQA_$C_{12}$ | >82% | >97 | >98 |

inhibited after three months water aging of the materials. Our study demonstrates 6 d efficacy of our QA_$C_{12}$ containing resins against bacterial adhesion and growth. Considering that most people brush their teeth to remove oral biofilm twice a day but will inevitably leave biofilm behind at random, difficult to reach sites, the ability of these surfaces to reduce oral biofilm formation over a time period of several days demonstrates that contact killing of adhering bacteria may be a clinically relevant way to prevent oral biofilm-related diseases. None of the contact-killing materials described in the literature are 3D printable, which makes our QA_$C_{12}$ containing resins new, offering many opportunities for developing antimicrobial objects for diverse applications (EPC Application No. 15167409.0-1454).

## 3. Conclusion

In summary, we have presented two general strategies to fabricate antimicrobial resins. Positively charged monomers with an appended alkyl chain are responsible for the antibacterial property and were either directly copolymerized with conventional resin components by photocuring or prepolymerized as a linear chain, which was then incorporated into a semi-interpenetrating polymer network by light-induced polymerization. Although both strategies yielded materials with minimal leaching of bioactives, the latter strategy resulted in polymer resins that exhibited the least leaching of the bioactive positively charged moieties possibly due to the formation of hydrogen- or covalent bonds between the cross-linked network and the antimicrobial polymer. The contact-killing abilities of the antimicrobial resins were even preserved upon coating of the materials with a salivary conditioning film, although incorporation of pQA_C12 in a polymer-incorporated SIPN resin yielded slightly less bacterial contact killing than copolymerizing QA_C12 directly in the resin. Therewith, the antimicrobial resins prepared can find application in dentistry as an adhesive, luting cement, or composite either to restore cavities or fix orthodontic brackets on teeth. With only little variation, both resin formulations were amenable to 3D printing with the prepolymerized QA polymer strategy yielding a more brittle material that has to be accounted for depending on the specific application aimed for. Complex geometries of oral appliances such as antimicrobial crowns or splints were successfully realized and the 3D printed objects exhibited mechanical properties that were almost identical to conventionally photocured polymer samples. The antimicrobial properties were shown to be caused by bacterial contact killing with the material rather than the release of antimicrobial compounds from the resin. Having optimized the activity and stability of these materials, we have a prototype at hand that is suited for further testing in a clinical setting, including not only dental applications but also, for instance, orthopedic ones like spacers and other polymeric parts used in total hip or knee arthroplasties. Moreover, the approach to developing 3D printable antimicrobial polymers can easily be transferred to other nonmedical application areas, such as food packaging, water purification, or even toys for children. To the best of our knowledge, the resins we developed represent the first report of an antimicrobial, contact-killing 3D printable material (EPC Application No. 15167409.0-1454).

## 4. Experimental Section

*Materials*: UDMA (mixture of isomers, ≥97%), CQ (97%), EDMAB (≥99%), 2-(dimethylamino)ethyl methacrylate (DMAEMA, 98%), GDMA (mixture of isomers, 85%), HEMA (97%), methacrylic acid (98%), *N,N′*-dicyclohexylcarbodiimide (99%), 4-cyano-4-(dodecylthiocarbonothioylthio)pentanoic acid (CDTA, 97%), 1-bromooctane (99%), 1-bromodecane (98%), 1-bromododecane (97%), and 1-bromohexadecane (97%) were purchased from Aldrich. 1-bromobutane (99%) and hydroquinone (ReagentPlus, ≥99.5%) were obtained from Sigma-Aldrich. All other chemicals including solvents were used as received.

*Synthesis of Quaternary Ammonium Methacrylate*: Quaternary ammonium methacrylate (QA_$C_n$) (see Scheme S3, Supporting Information) with alkyl chain lengths ($C_n$) in the range of $C_4$–$C_{16}$ were synthesized: 10 g of DMAEMA (63.6 mmol) and 67 mmol of alkyl bromides ($C_nH_{2n+1}Br$) were dissolved in 100 mL chloroform.[50] To inhibit self-polymerization of DMAEMA during quaternization, a small amount of hydroquinone (70 mg, 0.636 mmol) was added to the mixture. The reaction was conducted at 50 °C for 24 h, and then the solvent was evaporated under reduced pressure, followed by three times precipitation in a large excess of hexane. The precipitates were collected, redissolved in 20 mL of chloroform, and then passed through a layer of alkaline aluminum oxide to get rid of hydroquinone. The final product was obtained by removal of the solvent to give a white powder (yield: 89%). $^1$H NMR (400 MHz, $CDCl_3$): $\delta$ (ppm) = 0.91 (t, 3H, $N^+CH_2CH_2(CH_2)_{n-3}CH_3$), 1.40 (m, (2*n*–6)H, $N^+CH_2CH_2(CH_2)_{n-3}CH_3$), 1.75 (m, 2H, $N^+CH_2CH_2(CH_2)_{n-3}CH_3$), 1.93 (s, 3H, $CH_2C(CH_3)COO$), 3.49 (s, 6H, $CH_2N^+(CH_3)_2C_2H_2$), 3.68 (t, 2H, $N^+CH_2CH_2(CH_2)_{n-3}CH_3$), 4.15 (t, 2H, $COOCH_2CH_2N^+$), 4.65 (t, 2H, $COOCH_2CH_2N^+$), 5.66 and 6.12 (s, 2H, $CH_2C(CH_3)COO$).

*Synthesis of pQA*: First, tertiary amine (TA)-containing polymers were synthesized by RAFT copolymerizations of DMAEMA and HEMA in the presence of the chain transfer agent CDTA (Scheme S4, Supporting Information). In detail, CDTA (0.248 mol), DMAEMA (7.44 mol), HEMA (6.2 mol), and azobisisobutyronitrile (AIBN) (0.0496 mol) were dissolved in 10 mL of *N,N*-dimethylformamide (DMF) in a Schlenk flask, followed by five "freeze–pump–thaw" cycles to remove oxygen. Then the flask was filled with argon and sealed to allow polymerization at 65 °C for 12 h. Subsequently, the flask was cooled to room temperature and the viscous solution was precipitated in a large excess of diethyl ether to obtain the product in 70% yield. Afterward, quaternization of the above polymers was carried out using tenfold excess of alkyl bromides in relation to the nitrogen component. The reaction was conducted at 70 °C in DMF for 2 d and finally, the reaction mixture was precipitated in a large excess of *n*-hexane/diethylether (3/1, v/v). To fully remove the unreacted alkyl

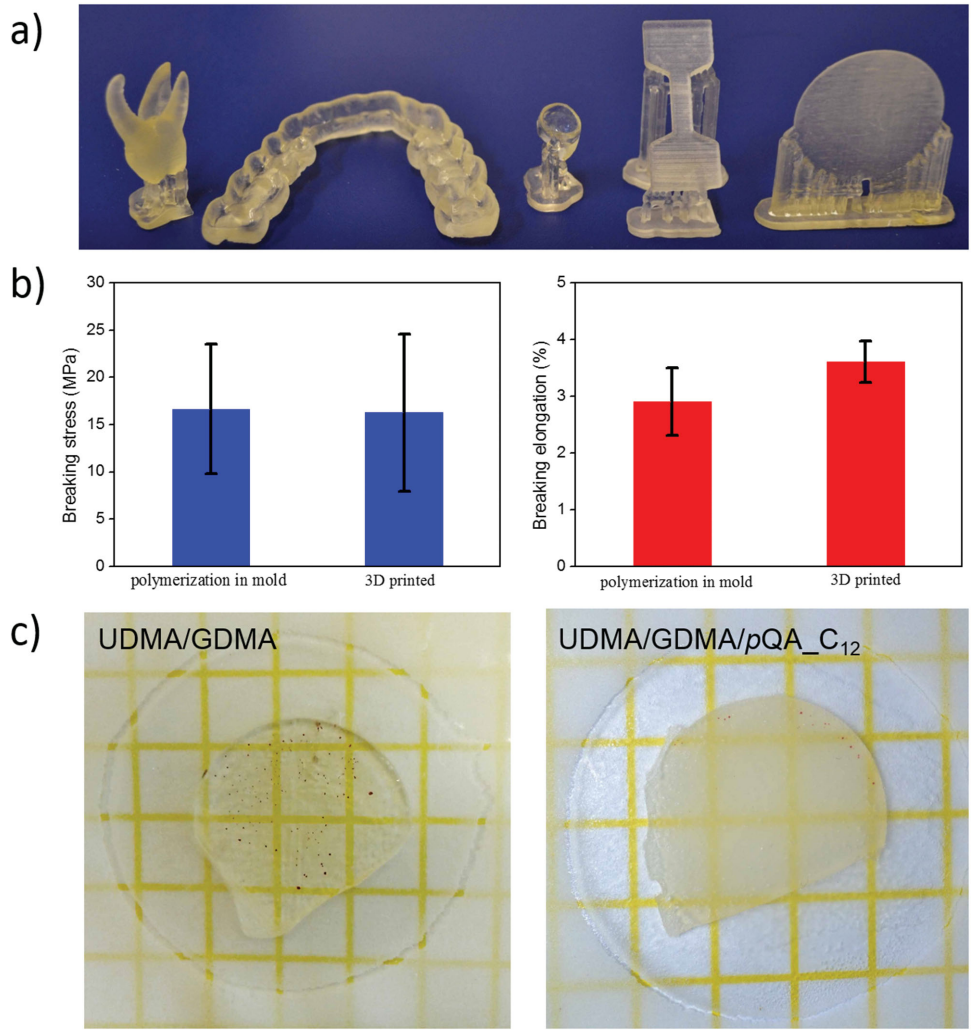


**Figure 6.** Object examples and properties of 3D printed, 25 wt% pQA_$C_{12}$ in a polymer-incorporated SIPN resin of UDMA/GDMA. a) 3D printed dental appliances or models (from left to right: molar tooth, clear splint, crown, tensile test bar, contact-killing test disc) based on polymerized positively charged compounds incorporated in an SIPN resin; b) tensile properties of 25 wt% pQA_$C_{12}$ in a polymer-incorporated SIPN system of UDMA/GDMA 3D printed tensile test bar and a test bar prepared in a polymerization mold by conventional photoillumination; and c) comparison of the contact-killing efficacy of a 3D printed 25 wt% pQA_$C_{12}$ in a polymer-incorporated SIPN system of UDMA/GDMA disc for *S. mutans* NS in the Petrifilm plate counting system with the one of a UDMA/GDMA disc (challenge number equals 30 CFUs $cm^{-2}$). Presence of CFUs (red dots) on the UDMA/GDMA disc versus the absence of CFUs on the UDMA/GDMA/QA_$C_{12}$ disc indicates that the bacterial contact-killing ability of the material is preserved upon 3D printing.

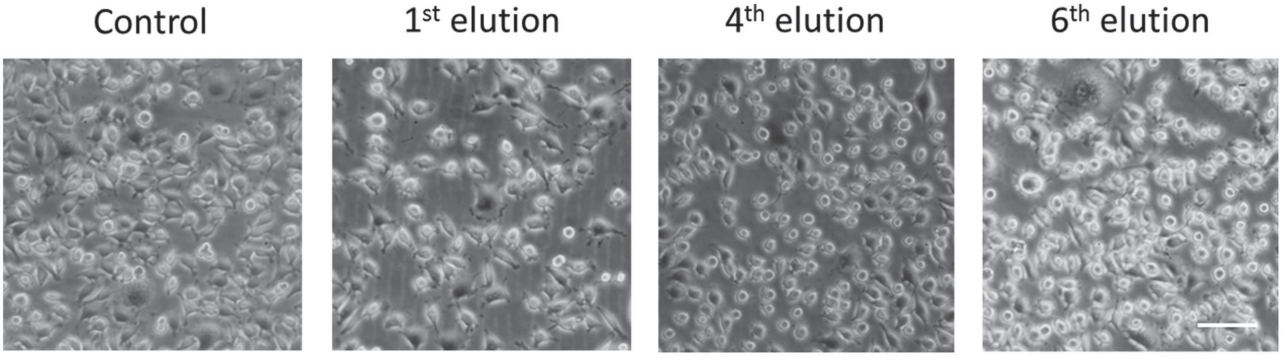


**Figure 7.** Biological consequences of leaching of pQA_$C_{12}$ from a polymer-incorporated SIPN resin of UDMA/GDMA. Morphology of fibroblast cells after growth in elution medium (see above). Well spread cells are indicating leaching of cytotoxic components including pQA_$C_{12}$ in cell-biologically negligible amounts.

bromides and monomers, the precipitated polymers were redissolved in ethanol, followed by dialysis against a solvent mixture of ethanol/acetone (10/1) for one week. The final products were obtained after evaporating the solvent remaining in the dialysis bags (cellulose membrane, cut-off molecular weight: 3.5 kD). A $^1$H NMR spectra (400 MHz, $d_6$-DMSO) of quaternized polymer is shown in Figure S1 (Supporting Information).

*Fabrication of QA_C$_n$-Containing Polymer Network*: Homogeneous resin mixtures containing 50 mol% of UDMA, 36 mol% of GDMA, and 14 mol% of QA_C$_n$ monomers were prepared by gentle sonication of the components at room temperature for 60 min. In order to initiate the polymerization under visible light, CQ (photoinitiator) and EDMAB (coinitiator) at an amount of 0.5 mol% in relation to the total amount of double bonds were added and sonication was performed for another 30 min to dissolve the photoinitiator and coinitiator. After that, a stainless steel mold (diameter: 20 mm; thickness: 0.5 mm) was filled with the viscous solutions and placed between two thin glass slides. The photocuring was carried out by vertical illumination of both sides of the polymerization mold at room temperature for 90 s, respectively, using a dental light source (Optilux 501, sds Kerr Sybron Dental Specialties, Middleton, WI, USA) with an irradiance of ≈1000 mW cm$^{-2}$. After photocuring, the sample surfaces were washed with isopropanol to remove unreacted monomers.

*Fabrication of Semi-Interpenetrating Polymer Network Incorporating pQA Polymers*: First, homogeneous mixtures containing 18 wt% of UDMA, 55 wt% of GDMA, and 25 wt% of pQA were prepared and then 1 wt% of CQ and EDMAB in relation to the total amount of double bonds was added, followed by sonication of the mixture for 1 h to form a clear solution. Subsequently, photocuring was carried out as described above. After photocuring, the sample surfaces were washed with isopropanol several times to remove unreacted monomers.

*3D Printing*: Two series of photocurable resin mixtures were prepared for 3D printing, requiring slight adjustment of the resin formulations described in the former two sections. To fit the laser wavelength of the stereolithographic printer (Formlabs Form 1), 1 wt% of bisacrylphosphine oxide photoinitiator (Ir819)[51] was added to the monomer mixture, instead of CQ and EDMAB. For 3D printing, several specially designed CAD models of dental restorations (i.e., molar teeth and crowns) and orthodontic retainers as well as specific dumbbell-shaped test bars for tensile tests and discs for the evaluations of contact-killing efficacies of the materials were sliced and each slice was projected onto the bottom layer of the resin tank of the printer. After transferring the resin mixtures into the resin tank, the printing process was started and a beam of UV light drew the object onto the surface of the liquid. Once a layer was completely traced and cured, the z-stage with the substrate was moved upward by 200 µm, covered with new resin and the next layer was cured. The resolution of the device was ≈300 µm in the *XY*-plane and 25 µm in the *Z*-direction. After all layers were printed, the printed objects were removed from the platform and washed with isopropanol to remove the adhering resin liquid. Finally, postprinting photocuring was carried out with models in a UV chamber for another 5 h.

*Mechanical Evaluations*: Tensile evaluations of dumbbell-shaped specimens were carried out to compare the mechanical properties of the materials fabricated by normal curing and 3D printing. The dimensions of the test geometries were the following: thickness: 2.0 mm; width: 4.5 mm; gauge length: 15 mm. The dumbbell-shaped specimens were clamped vertically between two holding grips and then the crosshead elongated the samples with a speed of 1 mm min$^{-1}$ until the specimen broke. As such breaking stress and strain% were recorded. Three parallel samples for each formulation were prepared.

*X-Ray Photoelectron Spectroscopy*: The quaternized nitrogen on the surface was determined by XPS. The instrument (S-probe; Surface Science Instruments, Mountain View, CA) was equipped with a monochromatic X-ray source (Al K$\alpha$ anode yielding 1486.8 eV X-rays), and was operated at 10 kV accelerating voltage and 22 mA filament current. The direction of the photoelectron collection angle was set to 35° with respect to the sample surface, and the electron flood gun was set at 10 eV. A survey scan was made with a 1000 × 250 µm$^2$ spot and a pass energy of 150 eV. Binding energies were determined by setting the binding energy of the $C_{1s}$ binding energy peak (carbon bound to carbon) at 284.8 eV. Detailed scans of the N1s binding energy peaks over a binding energy range of 20 eV were made using a pass energy of 50 eV. The N1s peak was subsequently decomposed in two fractions at 399.2 and 401.7 eV. The occurrence of a peak at 401.7 eV is indicative for the presence of charged nitrogen species[39] and was expressed in at% charged nitrogen species by multiplying the peak fraction at 401.7 eV with the total at% nitrogen.

*Contact Angle Measurements*: Water contact angles were measured on selected materials using the sessile drop method. Contact angles were calculated from droplet contours using a home-made contour monitor based on black and white thresholding.

*Determination of Monomer Conversion Rates Using Fourier-Transform Infrared Spectroscopy (FTIR)*: Polymerization kinetics were determined by FTIR using a Bruker IFS88 instrument. To this end, a small amount of monomer mixture was homogeneously spread between two KBr pellets to form a thin film. Next, the samples were irradiated for defined period of times (0, 2, 4, 6, 8, 10, 15, 20, and 30 s) with the dental light source (Optilux 501) and subsequently the FTIR spectra were recorded. The degree of conversion was obtained from the difference of peak areas at a wavelength of 1638 cm$^{-1}$ (CC stretching vibration) before and after polymerization.

*Contact Killing by Photocured Quaternary Ammonium Containing Resins Using 3M Petrifilm Aerobic Count Plates*: Gram-positive *S. mutans* NS, an own clinically isolated strain from the human oral cavity, causing dental caries, was used throughout this study. The strain was first streaked on a blood agar plate from a frozen stock and grown overnight at 37 °C. One colony was inoculated in 10 mL Todd Hewitt broth (THB, Oxoid, Basingstoke, UK) and incubated at 37 °C for 24 h. 10 mL of this culture was used to inoculate a main culture of 200 mL THB, which was incubated for 16 h at 37 °C. Bacteria were harvested by centrifugation for 5 min at 6500g and 10 °C and subsequently washed two times with buffer ($2 \times 10^{-3}$ M potassium phosphate, $50 \times 10^{-3}$ M potassium chloride, and $1 \times 10^{-3}$ M calcium dichloride, pH 6.8). Bacterial suspension concentrations of $10^4$, $10^5$, and $10^6$ bacteria mL$^{-1}$ were used to evaluate the contact killing of the coatings using a Petrifilm Aerobic Count plate (3M Microbiology, St. Paul, USA) at different challenge numbers. Contact-killing abilities of QA_$C_{12}$ and pQA_$C_{12}$ containing resins were evaluated in absence and presence of an adsorbed salivary film. To this end, human whole saliva from 20 volunteers of both genders was collected into ice-cooled cups after stimulation by chewing Parafilm and then pooled, centrifuged, dialyzed, and lyophilized for storage. Prior to lyophilization phenyl methyl sulfonyl fluoride was added to a final concentration of $1 \times 10^{-3}$ M as a protease inhibitor. Lyophilized saliva was reconstituted at 1.5 mg mL$^{-1}$ in buffer. Thus, reconstituted saliva will be referred to as "saliva." Volunteers gave their consent to saliva donation, in agreement with the Ethics Committee at UMCG (Approval No. M09.069162). Resin discs were sterilized using 70% ethanol and both discs with and without quaternary ammonium included were stored overnight in 2.5 mL saliva, taken out with a sterile tweezer, and the excess saliva was dripped off before placing the sample on the Petrifilm system. Bacterial suspension droplets ($10^4$, $10^5$, $10^6$ bacteria mL$^{-1}$) of 5 µL were subsequently added on bare resin discs and discs with an adsorbed salivary conditioning film, corresponding with a bacterial challenge number of 30, 300, and 3000 bacteria cm$^{-2}$, respectively.

A Petrifilm AC plate consists of two films, a bottom film containing standard nutrients, a cold-water gelling agent, and an indicator dye that facilitates colony counting, and a top film enclosing the sample within the Petrifilm system. The top layer of the Petrifilm was lifted to expose the substrate (plating surface) containing the gelling agent and 1 mL of sterilized demineralized water was added. Then the top film was slowly rolled down and a plastic "spreader" was used for even distribution of the liquid. After keeping the film at room temperature for 1 h to allow gelling, a sample disc was placed in between the two layers, followed by addition of 5 µL of an *S. mutans* NS suspension on the disc surface (diameter: 20 mm; thickness: 0.5 mm). After rolling down the top layer, Petrifilms were kept at 37 °C for 48 h. Finally, the number of colony forming units (naked eye–distinguishable red dots) was counted.

*Biofilm Inhibition by Photocured Resins with Quaternary Ammonium Compounds*: First, *S. mutans* was suspended in sterile buffer at a concentration of $3 \times 10^8$ mL$^{-1}$. Then, resin discs (for dimensions see above) were incubated with 3 mL of this bacterial suspension at 37 °C for 5 h, followed by exchange of the buffer with 3 mL of fresh THB medium. Next, the samples were incubated at 37 °C for another 6 d and growth medium was exchanged every 48 h. After that, each sample surface was stained with a mixture of SYTO 9 and propidium iodide dyes (LIVE/DEAD *Bac*Light Bacterial Viability Kits) at room temperature for 15 min in the dark for CLSM observations.

*UPLC-MS-Chemical Detection of Leakage*: Photocured resin discs constituted of UDMA/GDMA/QA_$C_{12}$ (14 mol%) were immersed in 4 mL of demineralized water at 37 °C for 6 d. Afterward, 200 µL of released medium was collected for UPLC-MS. Real-time UV signals were collected and each detectable peak (limit of detection for QA_$C_{12}$ was $100 \times 10^{-6}$ M) was measured by MS to confirm the target molecular weight of 326 g mol$^{-1}$.

*Cell Biological Consequences of Leakage*: Mouse fibroblasts NCTC-clone 929 (ATCC CCL-1) were grown in monolayer cultures in Dulbecco's modification of Eagle's medium supplemented with 4.5 g L$^{-1}$ D-glucose (DMEM/HG), 10% (v/v) fetal bovine serum, and $0.2 \times 10^{-3}$ M ascorbic acid-2-phosphate at 37 °C in a humidified atmosphere with 5% $CO_2$. At 95% confluence, fibroblasts were passaged using a trypsin-EDTA solution (Invitrogen, Breda, The Netherlands) and thus grown cells were used for cytotoxicity testing. Resin discs (surface area of 1 cm$^2$) were inserted in 100 mL cellular growth medium. Fibroblasts (10 000 cells mL$^{-1}$) were seeded (1 mL) in a 12-well plate and grown for 24 h. Growth medium was replaced every 24 h up to 6 d and each daily elution medium was used to grow fibroblasts for 24 h according to the above protocol after which cell growth was compared with 24 h growth in native 24 h culture medium using phase contrast microscopy.

*Microbiological Consequences of Leakage*: In order to determine whether elution media contained any antibacterial monomer or QA_$C_{12}$, a modified Kirby Bauer[47] test was carried out. A streptococcal culture was used to inoculate THB agar plates with a sterile cotton swab. 10 min after inoculation, 10 µL droplets of elution medium were placed in the center of each plate and plates were left to incubate for 48 h at 37 °C in ambient air, after which the width of the inhibition zones around the elution droplets was examined.

*Statistical Analysis*: Student's *t*-test was used to determine the statistical difference between various experimental and control groups. Differences at a level of $p < 0.05$ were considered statistically significant.

## Supporting Information

Supporting Information is available from the Wiley Online Library or from the author.

## Acknowledgements

This study was funded by the University Medical Center Groningen, The Netherlands. The authors would like to thank Dr. W. J. van der Meer from Department of Orthodontics, University Medical Centre Groningen for his expertise and assistance in 3D printing. H.J.B. is also director-owner of SASA BV. The authors declare no potential conflicts of interest with respect to authorship and/or publication of this article. Opinions and assertions contained herein are those of the authors and are not construed as necessarily representing views of the funding organizations or their respective employers. J.Y., P.Z., M.R.-A., M.v.d.L., and A.G. conducted the experiments; H.C.v.d.M. and H.J.B. contributed to antibacterial evaluation; A.H. supervised chemical experiments; Y.R. supervised 3D printing; J.Y., H.C.v.d.M., H.J.B., A.H., and Y.R. conceived the study design and analyzed the data; and J.Y., J.Y.G., H.C.v.d.M., H.J.B., A.H., and Y.R. wrote the paper.

Received: June 11, 2015
Revised: September 4, 2015
Published online: October 9, 2015

[1] B. Berman, *Bus. Horiz.* **2012**, *55*, 155.
[2] I. D. Ursan, L. Chiu, A. Pierce, *J. Am. Pharm. Assoc.* **2013**, *53*, 136.
[3] E. Dorey, *Chem. Ind.* **2014**, *78*, 7.
[4] N. Sandler, I. Kassamakov, H. Ehlers, N. Genina, T. Ylitalo, E. Haeggstrom, *Sci. Rep.* **2014**, *4*, 4020.
[5] J. Chimento, M. J. Highsmith, N. Crane, *Rapid Prototyping J.* **2011**, *17*, 387.
[6] T. M. Rankin, N. A. Giovinco, D. J. Cucher, G. Watts, B. Hurwitz, D. G. Armstrong, *J. Surg. Res.* **2014**, *189*, 193.
[7] S. V. Murphy, A. Atala, *Nat. Biotechnol.* **2014**, *32*, 773.
[8] J. S. Miller, K. R. Stevens, M. T. Yang, B. M. Baker, D. H. T. Nguyen, D. M. Cohen, E. Toro, A. A. Chen, P. A. Galie, X. Yu, R. Chaturvedi, S. N. Bhatia, C. S. Chen, *Nat. Mater.* **2012**, *11*, 768.
[9] M. S. Mannoor, Z. W. Jiang, T. James, Y. L. Kong, K. A. Malatesta, W. O. Soboyejo, N. Verma, D. H. Gracias, M. C. McAlpine, *Nano Lett.* **2013**, *13*, 2634.
[10] A. Atala, F. K. Kasper, A. G. Mikos, *Sci. Transl. Med.* **2012**, *4*, 160rv12.
[11] J. L. Silberstein, M. M. Maddox, P. Dorsey, A. Feibus, R. Thomas, B. R. Lee, *Urology* **2014**, *84*, 268.
[12] R. Van Noort, *Dent. Mater.* **2012**, *28*, 3.
[13] N. R. Silva, L. Witek, P. G. Coelho, V. P. Thompson, E. D. Rekow, J. Smay, *J. Prosthodontics* **2011**, *20*, 93.
[14] J. L. Erkal, A. Selimovic, B. C. Gross, S. Y. Lockwood, E. L. Walton, S. McNamara, R. S. Martin, D. M. Spence, *Lab Chip* **2014**, *14*, 2023.
[15] M. D. Symes, P. J. Kitson, J. Yan, C. J. Richmond, G. J. T. Cooper, R. W. Bowman, T. Vilbrandt, L. Cronin, *Nat. Chem.* **2012**, *4*, 349.
[16] B. Utela, D. Storti, R. Anderson, M. Ganter, *J. Manuf. Process.* **2008**, *10*, 96.
[17] D. B. Kolesky, R. L. Truby, A. S. Gladman, T. A. Busbee, K. A. Homan, J. A. Lewis, *Adv. Mater.* **2014**, *26*, 3124.
[18] K. Pataky, T. Braschler, A. Negro, P. Renaud, M. P. Lutolf, J. Brugger, *Adv. Mater.* **2012**, *24*, 391.
[19] L. E. Bertassoni, J. C. Cardoso, V. Manoharan, A. L. Cristino, N. S. Bhise, W. A. Araujo, P. Zorlutuna, N. E. Vrana, A. M. Ghaemmaghami, M. R. Dokmeci, A. Khademhosseini, *Biofabrication* **2014**, *6*, 024105.
[20] D. M. Monack, A. Mueller, S. Falkow, *Nat. Rev. Microbiol.* **2004**, *2*, 747.
[21] A. S. Chitnis, J. R. Edwards, P. M. Ricks, D. M. Sievert, S. K. Fridkin, C. V. Gould, *Infect. Control Hosp. Epidemiol.* **2012**, *33*, 993.
[22] Y. Ren, M. A. Jongsma, L. Mei, H. C. van der Mei, H. J. Busscher, *Clin. Oral. Investig.* **2014**, *18*, 1711.
[23] T. Wall, K. Nasseh, M. Vujicic, *U.S. Dental Spending Remains Flat Through 2012*, Health Policy Research Brief, American Dental Association, Chicago, IL, USA, January **2014**.
[24] A. Wiegand, W. Buchalla, T. Attin, *Dent. Mater.* **2007**, *23*, 343.
[25] P. W. Osinaga, R. H. Grande, R. Y. Ballester, M. R. Simionato, C. R. D. Rodrigues, A. Muench, *Dent. Mater.* **2003**, *19*, 212.
[26] B. A. Sevinc, L. Hanley, *J. Biomed. Mater. Res., Part B* **2010**, *94*, 22.
[27] K. Yamamoto, S. Ohashi, M. Aono, T. Kokubo, I. Yamada, J. Yamauchi, *Dent. Mater.* **1996**, *12*, 227.
[28] H. J. Sandham, L. Nadeau, H. I. Phillips, *J. Dent. Res.* **1992**, *71*, 32.
[29] A. Pepperney, M. L. Chikindas, *Probiotics Antimicro. Proteins* **2011**, *3*, 68.
[30] J. C. Tiller, C. J. Liao, K. Lewis, A. M. Klibanov, *Proc. Natl. Acad. Sci. USA* **2001**, *98*, 5981.
[31] C. J. Waschinski, J. Zimmermann, U. Salz, R. Hutzler, G. Sadowski, J. C. Tiller, *Adv. Mater.* **2008**, *20*, 104.
[32] D. Cui, A. Szarpak, I. Pignot-Paintrand, A. Varrot, T. Boudou, C. Detrembleur, C. Jérôme, C. Picart, R. Auzély-Velty, *Adv. Funct. Mater.* **2010**, *20*, 3303.
[33] A. Munoz-Bonilla, M. Fernandez-Garcia, *Prog. Polym. Sci.* **2012**, *37*, 281.

[34] G. Lu, D. Wu, R. Fu, *React. Funct. Polym.* **2007**, *67*, 355.
[35] B. Gottenbos, H. C. van der Mei, F. Klatter, P. Nieuwenhuis, H. J. Busscher, *Biomaterials* **2002**, *23*, 1417.
[36] P. Thebault, E. T. de Givenchy, R. Levy, Y. Vandenberghe, F. Guittard, S. Géribaldi, *Eur. J. Med. Chem.* **2009**, *44*, 717.
[37] C. J. Waschinski, J. C. Tiller, *Biomacromolecules* **2005**, *6*, 235.
[38] R. Liska, M. Schuster, R. Infuhr, C. Turecek, C. Fritscher, B. Seidl, V. Schmidt, L. Kuna, A. Haase, F. Varga, H. Lichtenegger, J. Stampfl, *J. Coat. Technol. Res.* **2007**, *4*, 505.
[39] P. G. Rouxhet, M. J. Genet, *Surf. Interface Anal.* **2011**, *43*, 1453.
[40] W. J. Loesche, *Microbiol. Rev.* **1986**, *50*, 353.
[41] J. Haldar, A. K. Weight, A. M. Klibanov, *Nat. Protoc.* **2007**, *2*, 2412.
[42] R. H. Fitzgerald, *Arch. Surg.* **1979**, *114*, 772.
[43] L. A. T. W. Asri, M. Crismaru, S. Roest, Y. Chen, O. Ivashenko, P. Rudolf, J. C. Tiller, H. C. van der Mei, T. J. A. Loontjens, H. J. Busscher, *Adv. Funct. Mater.* **2014**, *24*, 346.
[44] A. L. J. Olsson, P. K. Sharma, H. C. van der Mei, H. J. Busscher, *Appl. Environ. Microbiol.* **2012**, *78*, 99.
[45] C. Hansel, G. Leyhausen, U. E. Mai, W. Geurtsen, *J. Dent. Res.* **1998**, *77*, 60.
[46] C. Dawes, *J. Am. Dent. Assoc.* **2008**, *139*, 18S.
[47] R. O. Darouiche, J. Farmer, C. Chaput, M. Mansouri, G. Saleh, G. C. Landon, *J. Bone Jt. Surg.* **1998**, *80*, 1335.
[48] C. P. Fik, S. Konieczny, D. H. Pashley, C. J. Waschinski, R. S. Ladisch, U. Salz, T. Bock, J. C. Tiller, *Macromol. Biosci.* **2014**, *14*, 1569.
[49] S.-Q. Gong, D. J. Epasinghe, B. Zhou, L.-N. Niu, K. A. Kimmerling, F. A. Rueggeberg, C. K. Y. Yiu, J. Mao, D. H. Pashley, F. R. Tay, *Acta Biomater.* **2013**, *9*, 6964.
[50] J. He, E. Söderling, M. Österblad, P. K. Vallittu, L. V. Lassila, *Molecules* **2011**, *16*, 9755.
[51] U. Kolczak, G. Rist, K. Dietliker, J. Wirz, *J. Am. Chem. Soc.* **1996**, *118*, 6477.